IX International Conference on Particle-Based Methods
PARTICLES 2025
J. Bonet, M. Cremonesi, A. Franci, A. Gil (Eds)

SIMULATING INTERPARTICULAR FORCES IN CEMENTITIOUS MEDIA USING THE DISCRETE PARTICLE METHOD

F. Wiese*, R. Sposito*, A. Kustermann*, T. Stengel*

* Institute for Material and Building Research (IMB),
Munich University of Applied Sciences (HM)
Karlstraße 6, 80333 Munich, Germany
imb@hm.edu, www.imb.hm.edu

Key words: Concrete, Contact Model, Discrete Particle Method, Interparticular Forces

Abstract Concrete is by far the most produced material in the world, at around 15 billion tonnes per year [1]. Given the scale of production and the associated use of cement, the concrete industry is a large CO_2 emitter, responsible for more than twice the CO_2 emissions of global aviation [2, 3]. Consequently, concrete offers significant potential for climate impact mitigation by reducing the embodied CO_2 per kilogram of material [4]. Concrete consists mainly of sand, gravel, water, and Portland cement clinker, with the latter being the main source of its high global warming potential. Therefore, the ongoing research effort is to minimise the amount of clinker in concrete by pursuing two different strategies: the development of alternative binders and the optimisation of concrete composition. This study follows the latter approach. Optimising concrete composition requires a detailed understanding of the interparticular forces that occur. These forces are complex, and an efficient yet accurate strategy is required to predict and investigate their effects on small scales, with the aim of upscaling to concrete in the future. Therefore, this study investigates the linear viscoelastic contact model with adhesion forces to capture the interactions between cement clinker, limestone filler, and quartz sand in an alkaline solution. The contact model is then used to simulate the packing problem with three distinct materials. The resulting packing density is compared to the same simulation, without interparticular forces.

1 INTRODUCTION

Given concrete's significant carbon footprint due to the use of Portland cement clinker (PC), research is focusing on replacing and minimizing the amount of PC in concrete, while ensuring

the same quality. Concrete's primary mechanical property is the compressive strength. Typically, concretes compressive strength is predicted with the ratio of PC and water, the so-called w/c-ratio. However, since the beginning of the 20th century, researchers have been optimizing the proportioning of concrete [5] in order to improve its quality and strength. The aim is to match the grain sizes of the gravel and sand as closely as possible so that the fine sand fills all the voids in the coarse gravel. These voids are quantified by the packing density; in a system with no voids, the packing density is 1.0. The optimization of concretes proportioning is often used in ultra-high performance concrete (UHPC) and modern models for predicting the compressive strength consider the particle packing [6, 7]. For calculating the packing density models like the 3-parameter Particle Packing Model (3PPM) by Kwan [8], the Theoretical Packing Density Model (TPDM) by Roqier [9] or the Compressive Packing Model (CPM) by De Larrard [6] are available. These Models only consider the geometrical effects shown in Figure 1.

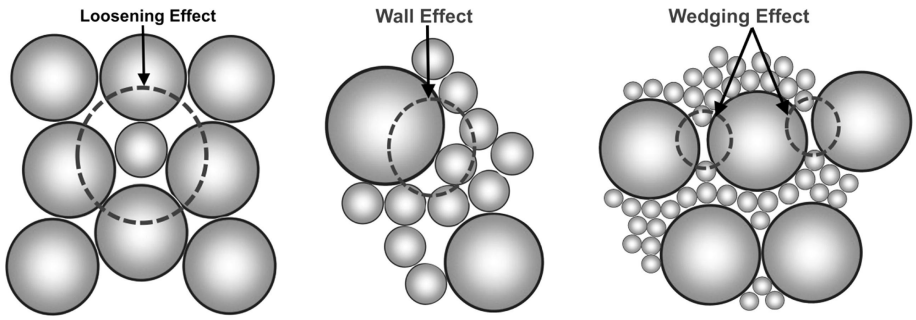

Figure 1: Geometrical effects, from [10]

For non-cohesive particles, these models predict the packing density well, but cohesive particles, like fine PC, behave very differently [10]. Fine particles with a high specific surface area are more influenced by surface related forces rather than gravitational forces. In particular, Van der Waals (VdW) forces and the electrostatic double layer (EDL) outweigh the gravitational forces in cementitious media [11]. Simulations utilizing the Discrete Particle Method (DEM) give insights into the resulting packing density and particle arrangement with adhesion forces [12]. Therefore, this paper investigates the linear viscoelastic contact model for considering mentioned forces with polydisperse micro-particles (radius 0.5 µm – 7.0 µm).

2 INTERPARTICULAR FORCES

2.1 Van der Waals forces

Van der Waal (VdW) forces are complex intermolecular interactions. They occur between permanent dipoles as well as induced dipoles, caused by fluctuations in the charge distribution within the electron shell of molecules. The surface-related VdW energy is calculated using the Hamaker constant and a geometrical term as shown in Equation (1) [13].

$$G_{VdW} = -A \cdot H \tag{1}$$

In cementitious media, the pore solution forms immediately after PC and water are mixed. It is an electrolyte with high ionic strength. Therefore, both shielding and retardation effects occur: shielding affects the zero-frequency part, whereas retardation influences the frequency-dependent portion. Using Flatts [11] retardation function, which depends only on the particle distance, the energy is calculated using Equation (2).

$$G_{vdW} = -A \cdot f_R(h_v) \cdot H \tag{2}$$

When particle 1 interacts with particle 2 through the medium (pore solution) 3, the Hamaker constant is calculated using Equation (3), the retardation function using Equation (4) and the geometrical term is described in Equation (5).

$$\begin{aligned} A =& \frac{3}{4} kT \left(\frac{\varepsilon_{0,1} - \varepsilon_{0,3}}{\varepsilon_{0,1} + \varepsilon_{0,3}} \right) \left(\frac{\varepsilon_{0,2} - \varepsilon_{0,3}}{\varepsilon_{0,2} + \varepsilon_{0,3}} \right) \\ &+ \frac{3 h_P \nu_{UV}}{8\sqrt{2}} \frac{(n_1^2 - n_3^2)(n_2^2 - n_3^2)}{(n_1^2 + n_3^2)^{1/2} (n_2^2 + n_3^2)^{1/2} \left[(n_1^2 + n_3^2)^{1/2} + (n_2^2 + n_3^2)^{1/2} \right]} \end{aligned} \tag{3}$$

$$f_R(h_v) = (m_1 h_v^2 + m_2 h_v + m_3) \cdot \exp(-m_4 h_v) + m_5 \cdot \exp(-m_6 h_v) \tag{4}$$

$$\begin{aligned} H = \frac{1}{6} \Bigg[& \frac{2R_1R_2}{h_v^2 + 2(R_1+R_2)h_v} + \frac{2R_1R_2}{h_v^2 + 2(R_1+R_2)h_v + 4R_1R_2} \\ & + \ln \left(\frac{h_v^2 + 2(R_1+R_2)h_v}{h_v^2 + 2(R_1+R_2)h_v + 4R_1R_2} \right) \Bigg] \end{aligned} \tag{5}$$

A	Hamaker constant [J]	k	Boltzmann constant [J/K]
T	Temperature [K]	h_P	Planck constant [J·s]
ν_{UV}	Characteristic UV frequency [Hz]	$\varepsilon_{0,i}$	Static permittivity [–]
n_i	Refractive index in the visible range [–]		
m_1	$0.00017E$-9	m_2	$-0.01163E$-9
m_3	$0.92551E$-9	m_4	$0.03237E$-9
m_5	$0.08743E$-9	m_6	$0.00270E$-9
h_v	Distance [m]	R_i	Radius [m]

The derivative of the surface-related energy with respect to the particle distance yields the resulting force, see Equation (6) [13].

$$F_{VdW} = -\frac{dG_{vdW}}{dh_v} = A \left(f_R \frac{dH}{dh_v} + H \frac{df_R}{dh_v} \right) \tag{6}$$

2.2 Electrostatic double layer

When particles with surface charge are dissolved in electrolytic solution, the ions from the electrolyte accumulate on the particle surface. The electrostatic double layer (EDL) forms. It consists of a fixed layer, where the ions can not move and a diffuse layer, where ions can move. When the diffuse layers of two particles overlap, an osmotic pressure is exerted between them. Assuming a constant potential at the particle surfaces, this pressure can be described by Equation (7) [13].

$$P = 2\varepsilon_0 \varepsilon \kappa^2 \psi_{(0)}^2 \exp(-\kappa D) \tag{7}$$

The integration over the distance gives the surface-related energy. Using the Derjaguin approximation, the force between two spheres can be calculated with Equation (8) [13].

$$F_{EDL} = 2\pi a W = 4\pi a\, \varepsilon\, \varepsilon_0\, \kappa\, \psi_0^2\, exp(-\kappa D) \tag{8}$$

$$a = \frac{R_1 R_2}{R_1 + R_2} \qquad I = \frac{1}{2}\sum_i c_i z_i^2 \qquad \kappa = \sqrt{\frac{2e^2 N_\mathrm{A} \cdot I}{\varepsilon \varepsilon_0 k T}}$$

ε	Relative permittivity pore solution [–]	ε_0	Permittivity vacuum [C^2/(N·m^2)]
κ	Debye parameter [1/m]	ψ_0	Surface potential [V]
D	Distance [m]	R	Radius [m]
c	Ion concentration [mol/m^3]	z	Ion valence [–]
e	Elementary charge [C]	N_A	Avogadro constant [1/mol]
k	Boltzmann constant [J/K]	T	Temperature [K]

2.3 Superposition

VdW forces and the EDL are acting simultaneously in cementitious media and must therefore be considered in superposition. However, the relevant particle distances for VdW and EDL interactions are not identical. VdW forces originate from electron interactions within the particle, whereas EDL forces arise from the fixed layer around the particle. Consequently, these distances require correction from the surface-to-surface distance d. Assuming adsorption of monovalent calcium with a atomic radius of 123 pm, the fixed layer can be estimated at approximately 0.25 nm. Therefore, particle distance for the EDL needs to be reduced with Equation (9).

$$D = d - 2.5 \cdot 10^{-10} \quad [m] \tag{9}$$

The distance from the atomic nucleus to the particle surface can be estimated by the atomic radius of approximately 0.1 nm. Accordingly, the interparticle distance for the VdW interaction is increased as shown in Equation (10).

$$h_v = d + 1 \cdot 10^{-10} \quad [m] \tag{10}$$

In addition, since PC particles are non-spherical, the contact radius relevant for interparticle forces is smaller than the actual particle radius (see Figure 2). Therefore, the radius must be reduced when calculating the surface-related forces, as described in Equation (11) [14].

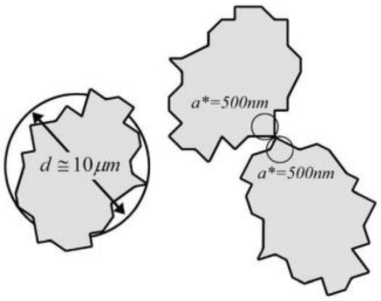

Figure 2: Contact radius, from [14]

$$R_c = \frac{R}{10} \tag{11}$$

Considering both the adhesive VdW force and the repulsive EDL force in cementitious media, the total interaction force emerges according to Equation (12).

$$F_{adh} = F_{vdw} - F_{EDL} \tag{12}$$

3 HYDRODYNAMIC INTERACTIONS

Particles suspended in a liquid phase interact not only with each other but also with the surrounding fluid. In this study, only viscous damping is considered, as expressed by Equation (13).

$$F_v = 6\pi\eta_F R v \tag{13}$$

η_F Viscosity [Pa s] R Radius [m]
v Velocity [m/s]

4 CONTACT MODEL

4.1 Mathematical formulation

The investigated contact model is based on the Hertzian contact formulation with spring stiffness k, damping coefficient γ and an adhesive force F_{adh} acting in normal direction, as shown in Equation (14). The adhesive force results form the superposition of the VdW and

EDL-forces according to Equation (12) and therefore depends on material parameters as well as the interparticle distance or overlap.

$$F_{\mathrm{n}} = k_{\mathrm{n}}\,\delta - \gamma_{\mathrm{n}}\,v_{\mathrm{rel}}^{\mathrm{n}} - F_{adh}(\delta) \quad \text{if } \delta > 0 \tag{14}$$

In one dimension, the corresponding equation of motion is given by Equation (15).

$$\ddot{\delta} + \frac{\gamma}{m_{eff}}\dot{\delta} + \frac{k}{m_{eff}}\delta = \frac{F_{adh}(\delta)}{m_{eff}} \quad \text{with} \quad m_{eff} = \frac{m_1\,m_2}{m_1 + m_2} \tag{15}$$

Defining the damping factor η according to Equation (16) and the eigenfrequency ω_0 according to Equation (17), the equation of motion simplifies to Equation (18).

$$2\eta = \frac{\gamma}{m_{eff}} \tag{16}$$

$$\omega_0^2 = \frac{k}{m_{eff}} \tag{17}$$

$$\ddot{\delta} + 2\eta\,\dot{\delta} + \omega_0^2\,\delta = \omega_0^2\,\delta_{eq} \tag{18}$$

With adhesion forces, an equilibrium overlap δ_{eq} at t_∞ arises, depending on the spring stiffness and the adhesion force, see Equation (19).

$$\delta_{eq} = \frac{F_{adh}}{k} \tag{19}$$

Substituting δ to $x_{(t)} = \delta_{(t)} - \delta_{eq}$, gives Equation (20).

$$\ddot{x_{(t)}} + 2\eta\dot{x_{(t)}} + \omega_0^2\,x_{(t)} = 0 \tag{20}$$

For the system to be underdamped, Equation (21) must be satisfied.

$$w_0 > \eta \tag{21}$$

For an underdamped system, Equation (20) can be solved according to Equation (22)

$$x_{(t)} = \exp(-\eta t)\left(x_0 \cdot \cos(wt) + \frac{v_0 + \eta\,x_0}{\omega}\sin(\omega t)\right) \tag{22}$$

To solve for the overlap from $\delta_0 = 0$, the initial conditions are set to $x_0 = -\delta_{eq}$ and $\tau = t - t_0$. This yields Equation (23).

$$\delta_{(\tau)} = \delta_{eq}\left[1 - \exp(-\eta\,\tau)\left(\cos(\omega\,\tau) + \frac{\eta}{\omega}\sin(\omega\,\tau)\right)\right] + \frac{v_0}{\omega}\exp(-\eta\,\tau)\sin(\omega\,\tau) \tag{23}$$

The resulting overlap function for $R_{12} = 8.11 \cdot 10^{-7}$ m, $k_n = 6.57 \cdot 10^{-6}$ N/m, $\gamma_n = 3.11 \cdot 10^{-12}$, $m_{1,2} = 2.288 \cdot 10^{-18}$ m and $v_0 = 1 \cdot 10^{-}$ m/s is visualized in Figure (3).

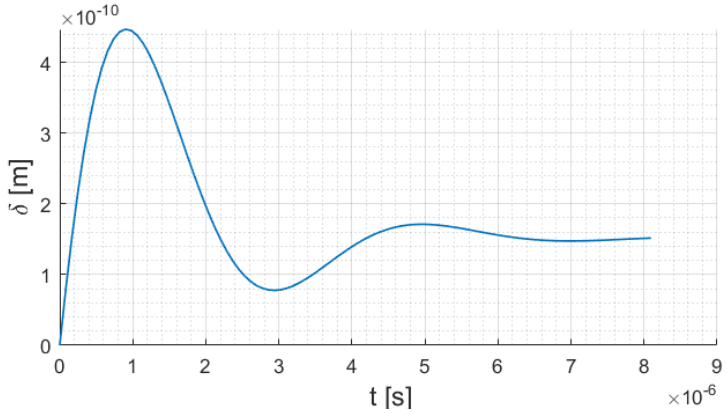

Figure 3: Overlap over time

4.2 Numerical stability

The required timestep to ensure numerical stability is often estimated from the collision time of two interaction particles. For the Hertzian contact model without adhesion, the collision time is obtained by solving the equation of motion for the overlap and evaluating the first zero crossing in the underdamped case, as given in Equation (24).

$$t_c = \frac{\pi}{\sqrt{w_0^2 - n^2}} \tag{24}$$

In the presence of adhesion, the contact time formally tends to infinity. Nevertheless, Equation (24) can still be used to estimate a stable timestep. To avoid unrealistically large overlaps, the equilibrium overlap is limited in this study to one fourth of the smallest radius in the interaction R_{min} according to Equation (25).

$$\delta_{eq} = \frac{1}{4} R_{min} \tag{25}$$

Using the relationship between adhesive force and spring stiffness from Equation (19), the minimum effective spring stiffness in the interaction can be calculated using Equation (26).

$$k_{min}^{eff} = 4 \frac{F_{adh}}{R_{min}} \tag{26}$$

For a given normal coefficient of restitution ε_n, particle mass m and spring stiffness k_n, the damping coefficient is given by Equation (27).

$$\gamma_n = \frac{\sqrt{(mk_n)}}{\pi^2 + (\log(\varepsilon_n))^2 \cdot \log(\varepsilon_n)} \tag{27}$$

With the minimum effective spring stiffness from Equation (26) and the damping coefficient from Equation (27), the stable time step can be obtained from Equation (28), using the safety coefficient c.

$$\Delta t = \frac{1}{c} \cdot t_c = \frac{1}{c} \cdot \frac{\pi}{\sqrt{(w_0^2 - \eta^2)}} = \frac{1}{c} \cdot \frac{\pi}{\sqrt{\left[\frac{k_n}{m_e ff} - \left(\frac{\gamma_n}{2m_{eff}}\right)^2\right]}} \tag{28}$$

5 SIMULATING PACKING PROBLEM

5.1 Software

For the following simulations, MercuryDPM [15] is used. MercuryDPM utilizes the Verlet algorithm to solve Newton's laws of motion. Simulations can be parallelised using MPI via dividing the simulation domain into subdomains as well as with openMP via shared-memory jobs.

5.2 Setup

In the packing simulation, 6,995 polydisperse particle are falling into a box. Particle radii range from approximately 0.8 to 7.5 μm, are randomly distributed with a minimum initial separation of 10 nm to prevent initial agglomeration. Three distinct materials are implemented. The material-dependent coefficients as well as the global coefficients are summarized in Table (1). The geometrical setup can be seen in Figure (5). The contact model according to Equation (14) is used. The adhesive force, according to Equation (12) is calculated with the attractive VdW force according to Equation (6) and the repulsive EDL force according to Equation (8). In every interaction, the stiffness is calculated using Equation (26) and the dissipation using Equation (27) with a restitution coefficient of 0.01. A timestep of $4 \cdot 10^{-8}$ s was used for a simulation time of 4 s. Eight OpenMP threads were used. Under the influence of the adhesive force, gravity and the viscous damping according to Equation (13), particles settle into the box. The same simulation is repeated with no acting adhesive force.

5.3 Results

After the simulation, the box was subdivided into seven height levels. For each height level, the packing density was calculated. In the case without adhesion, the upper levels were not sufficiently filled with particles therefore only the first three height levels are compared in Figure (4). As can be seen, the packing density is considerably lower when interparticle forces are taken into account, approximately half that obtained when interparticle forces are neglected. Snapshots of the simulation are visualized in Figure (5).

Table 1: Material and physical coefficients

	Material 1	Material 2	Material 3
Number of particles	6.479	470	46
ρ [kg/m^3]	3267	2784	2600
ψ [V]	0.049	0.015	0.016
ε [–]	3.80	3.30	1.55
n [–]	1.68	1.60	2.00
T [K]		293.15	
I [mol/m^3]		684	
ε_3 [–]		60.35	
n_3 [–]		1.34	
ν_{UV} [s^{-1}]		$3.0 \cdot 10^{15}$	

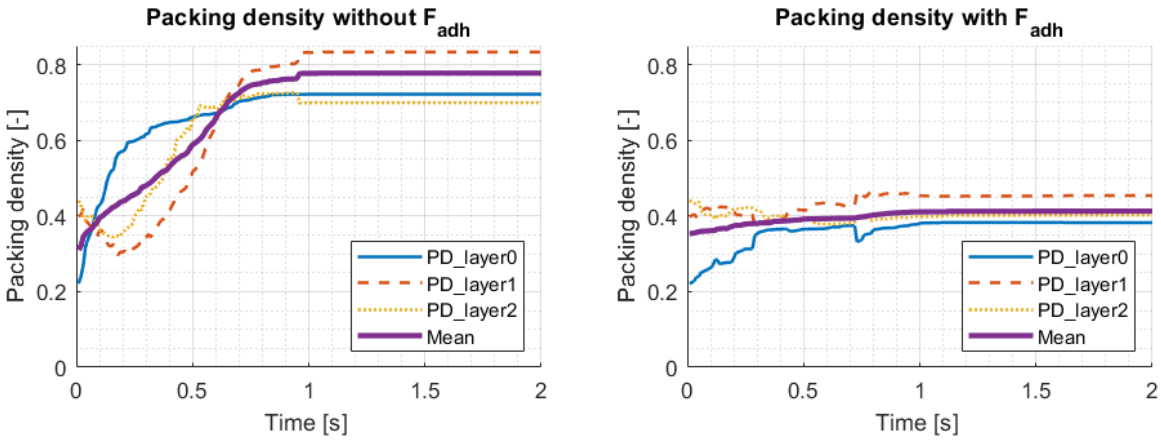

Figure 4: Packing densities with and without F_{adh}

6 CONCLUSIONS

This paper investigated a linear viscoelastic contact model to capture interparticular forces in cementitious media with polydisperse micro-particles (radius 0.5 µm – 7.0 µm) in a packing simulation. A minimum effective stiffness and a corresponding timestep criterion were derived to ensure numerical stability and applied in the simulations. The results show that considering adhesive forces reduces the packing density by about half, highlighting their strong influence on microstructure. While the model is suitable for simulating interparticle forces, the required limitation of stiffness leads to very small timesteps and high computational cost. Future work should focus on strategies to scale forces and particle properties to enable efficient upscaling to mortar and concrete systems.

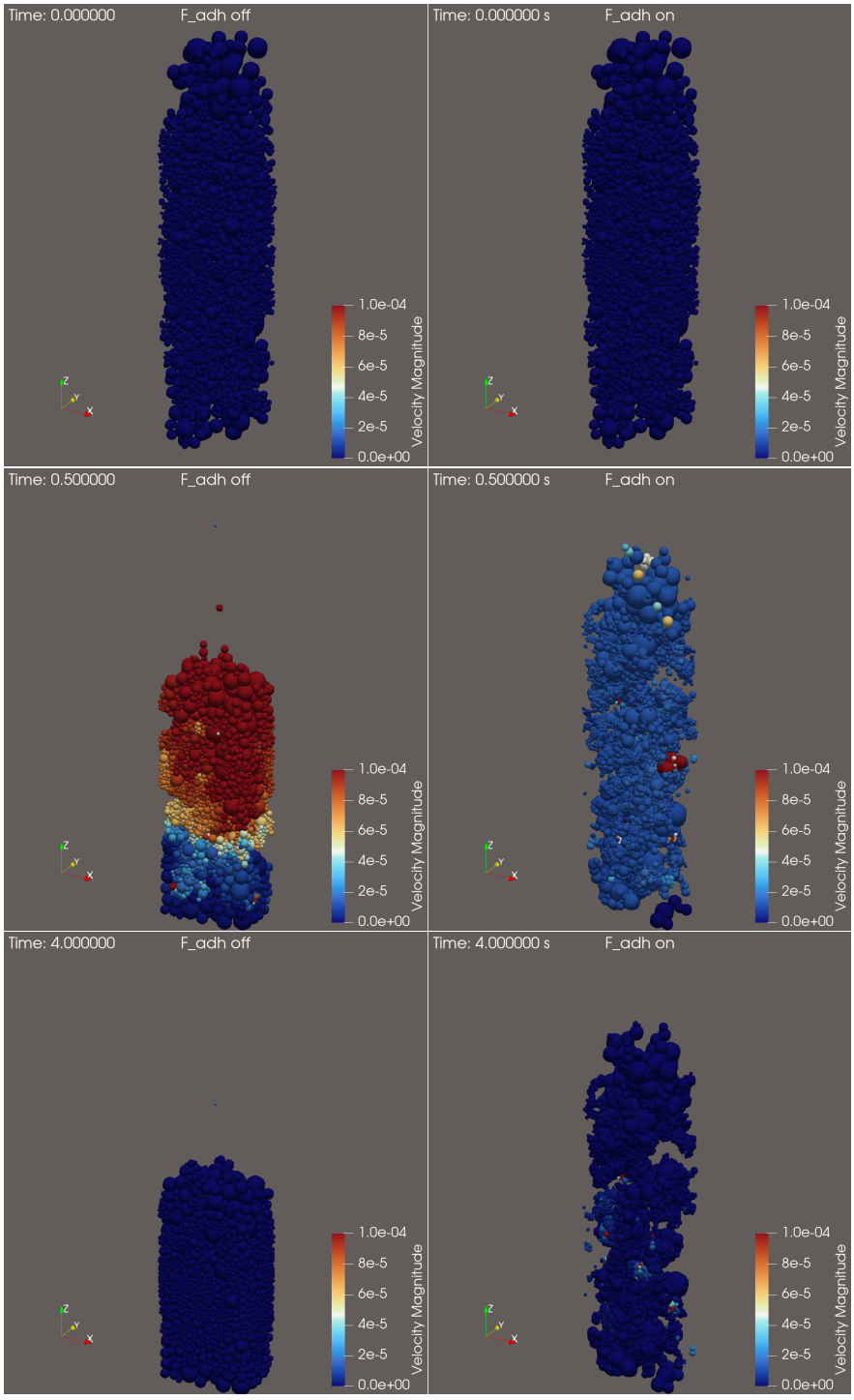

Figure 5: Snapshots of the simulations

REFERENCES

[1] Ashby, M. F. Materials and the Environment. Elsevier. (2021).

[2] Global Carbon Project. *Carbon dioxide emissions from the manufacture of cement worldwide from 1960 to 2023 (in million metric tons)*. Publisher: Statista. 2023.

[3] EDGAR/JRC. *Carbon dioxide emissions from international aviation worldwide from 1970 to 2023 (in million metric tons)*. Publisher: Statista. 2024.

[4] Barcelo, L. et al. Cement and carbon emissions. *Mater Struct* (2014) **47**:1055–1065. https://doi.org/10.1617/s11527-013-0114-5.

[5] Fuller, W. B. and Thompson, S. E. The Laws of Proportioning Concrete. *T. Am. Soc. Civ. Eng.* (1907) **59**:67–143. https://doi.org/10.1061/TACEAT.0001979.

[6] De Larrard, F. Concrete Mixture Proportioning. CRC Press. (1999).

[7] Chidiac, S. E., Moutassem, F., and Mahmoodzadeh, F. Compressive strength model for concrete. *Magazine of Concrete Research* (2013) **65**:557–572. https://doi.org/10.1680/macr.12.00167.

[8] Kwan, A., Chan, K., and Wong, V. A 3-parameter particle packing model incorporating the wedging effect. *Powder Technology* (2013) **237**:172–179. https://doi.org/10.1016/j.powtec.2013.01.043.

[9] Roquier, G. A Theoretical Packing Density Model (TPDM) for ordered and disordered packings. *Powder Technology* (2019) **344**:343–362. https://doi.org/10.1016/j.powtec.2018.12.033.

[10] Mehdipour, I. and Khayat, K. H. Understanding the role of particle packing characteristics in rheo-physical properties of cementitious suspensions: A literature review. *Construction and Building Materials* (2018) **161**:340–353. https://doi.org/10.1016/j.conbuildmat.2017.11.147.

[11] Flatt, R. J. Dispersion forces in cement suspensions. *Cement and Concrete Research* (2004) **34**:399–408. https://doi.org/10.1016/j.cemconres.2003.08.019.

[12] Parteli, E. J. R. et al. Attractive particle interaction forces and packing density of fine glass powders. *Sci Rep* (2014) **4**:6227. https://doi.org/10.1038/srep06227.

[13] Israelachvili, J. N. Intermolecular and surface forces. Academic press. (2011).

[14] Roussel, N. et al. Steady state flow of cement suspensions: A micromechanical state of the art. *Cement and Concrete Research* (2010) **40**:77–84. https://doi.org/10.1016/j.cemconres.2009.08.026.

[15] Weinhart, T. et al. Fast, flexible particle simulations — An introduction to MercuryDPM. *Computer Physics Communications* (2020) **249**:107129. https://doi.org/10.1016/j.cpc.2019.107129.